IOP Publishing New J. Phys. 22 (2020) 093066 https://doi.org/10.1088/1367-2630/abb54c

New Journal of Physics

The open access journal at the forefront of physics

Deutsche Physikalische Gesellschaft DPG

IOP Institute of Physics

Published in partnership with: Deutsche Physikalische Gesellschaft and the Institute of Physics

OPEN ACCESS

RECEIVED
26 July 2020

REVISED
2 September 2020

ACCEPTED FOR PUBLICATION
4 September 2020

PUBLISHED
21 September 2020

PAPER

Density functional theory studies of hydrogen bonding vibrations in sI gas hydrates

Hao-Cheng Wang[1], Xu-Liang Zhu[1], Jing-Wen Cao[1], Xiao-Ling Qin[1], Ye-Chen Yang[2], Tian-Xiao Niu[3], Ying-Bo Lu[1] and Peng Zhang[1]

[1] School of Space Science and Physics, Shandong University, West Wenhua Road No. 180, Weihai, Shandong, 264209, People's Republic of China

[2] Department of Physics, Southern University of Science and Technology, Xueyuan Avenue No. 1088, 518055 Shenzhen, People's Republic of China

[3] Girton College, University of Cambridge, Huntingdon Road, Cambridge, CB3 0JG, United Kingdom

* Author to whom any correspondence should be addressed.

E-mail: zhangpeng@sdu.edu.cn

Keywords: hydrogen bonding, gas hydrates, phonons, DFT

Supplementary material for this article is available online

Abstract

To analyze the vibrational modes of water and methane in structure I gas hydrates, we constructed a 178-atom supercell with two small cages of type 5^{12} and six large cages of type $5^{12}6^2$. We applied the density functional theory method to simulate the vibrational spectrum and normal modes of methane hydrates. In accord with our previous studies, we confirmed that two groups of hydrogen bond (H-bond) peaks (at around 291 and 210 cm^{-1}) in the translational bands come from two kinds of intermolecular H-bond vibrational modes. This is the first investigation of H-bond vibrations in methane hydrates. The partial modes of CH_4 were extracted. We found that the CH_4 phonons in the translational region are below 180 cm^{-1} so that the influence of methane on the H-bond is insignificant. We proposed a new method to decompose gas hydrates via direct application of terahertz radiation to the H-bonds. Herein, we confirmed that CH_4 molecules do not absorb this energy.

1. Introduction

With the depletion of oil and coal, gas hydrates will play a vital role in energy use and environmental protection. Sloan [1] estimated that the current energy reserves of methane hydrates are twice the total fuel fossil reserves, Lunine and Stevenson [2] wrote that methane hydrates make up the major satellite nebulae. And Takeya *et al* [3] revealed that the potential of methane hydrate used in actual methane storage. In addition, solutions to the blockage of methane hydrates in natural gas pipelines [4] and the accelerating effects of climate change [5] are highly valued. Traditional methods for extraction of natural methane hydrates include thermal stimulation, pressure reduction, and catalysts. However, commercial exploitation has not yet been realized due to economic and safety factors [6, 7]. Therefore, it is imperative to develop an efficient and sustainable method to dissociate methane hydrates.

Gas hydrates are crystalline solids that are often composed of cage-like structures of host molecules surrounding various nonpolar guest molecules. Gas hydrates are divided into various structures according to the cage numbers and cage types. Among these, structure I (sI) is the most common structure found in nature, first presented by Muller and von Stackelberg in 1951 [8], in which methane constitutes the overwhelming majority of guest molecules [9]. Hoshikawa *et al* [10] examined hydrogen of deuterated methane hydrate by means of the neutron powder diffraction data. An sI-type crystal comprises two small cages of type 5^{12} (pentagonal dodecahedrons) and six large cages of type $5^{12}6^2$ (a type of tetrakaidecahedral cavity), and only small molecules (0.4–0.55 nm) [11] such as methane and carbon dioxide can be encaged.

Water molecules are entrapped into cages by hydrogen bonding, whereas the host and guest molecules are connected by van der Waals forces.

Ice XVII, one kind of sI-type lattice, is derived from the phase diagram of the first H_2–H_2O compounds prepared in the laboratory [12, 13]. Ice XVII has the same structural definition as sI: a composition of pentagons linked with other pentagons via shared vertices [14]. For sI, two additional hexagons are required to maintain the hydrogen-bond strain. However, ice XVII can only form pentagons and therefore adopts a pipe structure rather than a cage structure like sI.

Since Anthonsen [15] first presented the Raman scattering spectroscopy of halogen hydrates, many researchers have focused on the effects of encapsulated methane in the band of C–H stretching via Raman spectroscopy [15–17]. Sum *et al* [16] first assigned the peaks at 2905 and 2915 cm^{-1} to the large cage and small cage, respectively. The two peaks' intensity ratio of 3:1 was interpreted as the number ratio of these two cages. This phenomenon in the vibrational spectrum was also confirmed by Greathouse *et al* [17]. In another study, Kortus *et al* [18] used melanophlogite, which has the same framework structure as sI, to discuss the influence of structure on the Raman spectrum of methane.

In contrast, Schicks *et al* [19] explored the influence of host molecules by Raman spectroscopy rather than guest molecules and found similarities in the spectra between sI and ice Ih in O–H stretching and H-bond translational vibrations. Hanson and Berg [20] indicated that metastable methane hydrates must have the ability to exist in different cavities. Tulk *et al* [21] compared the host lattice of methane hydrates with ice Ih in the region of coupled O–H vibrations.

In theoretical simulations, John [22] simulated the sI structure with an *ab initio* method to explore the relationship between the stretching vibrational frequencies and the CH bond length. Ramya *et al* [23] investigated the effects of methane in large and small cages, and the properties of empty cages.

Although many experimental and theoretical studies of methane hydrates have been carried out, the molecular vibrations in the far-infrared (IR) region have yet to be investigated due to the complexities of mixed host and guest phonons. From the view of physics, to explore an efficient method of the exploitation of gas hydrates for energy purposes, one should investigate the interactive mechanisms of H-bonds inside them.

In this study, we simulated the vibrational modes of H-bonds in sI methane hydrates. We present the calculated IR and Raman spectra and phonon density of states (PDOS). Compared with ice XVII, an sI-type clathrate hydrate without guest molecules [24], the encapsulation of methane was found to have little effect on H-bonds. This finding confirmed our prediction that a new method for the dissociation of gas hydrates could be explored [25].

2. Computational details

We performed calculations on sI methane hydrates using the CASTEP [26] code, a first-principles density functional theory module in the Materials Studio platform. The first difficult task was to construct a hydrogen disordered sI crystal structure, a supercell with 178 atoms. We generated several zero-total-dipole-moment sI clathrate hydrate structure files by GenIce [27] script with various random seeds. We then selected the structure that possessed the most even distribution for this study. The structure is illustrated in a supplementary file (https://stacks.iop.org/NJP/22/093066/mmedia) of supporting information.

We chose the revised Perdew–Burke–Ernzerhof functional [28], a generalized gradient approximation exchange–correlation functional, for the quantum mechanics calculation. The self-consistent field and energy tolerance was set at 1.0×10^{-9} eV/atom. The energy cutoff was set at 750 eV, and we calculated the $\omega(q)$ relationship at the gamma point. The reduced Brillouin zone of a large supercell is very small, resulting in a tiny $\omega(q)$ dispersion. The norm-conserving pseudopotential was used for calculation of phonons. The hydrostatic pressure was set at 1 MPa.

3. Results and discussion

Figure 1 depicts the simulated spectra of Raman, IR, PDOS (sI), and PDOS (CH_4), and the correlated data are listed in table 1. Theoretically, the optical vibrational modes are all Raman and IR active due to disordered hydrogen. Due to the broad scale of the intensity in various regions, we adjusted their proportions and displayed the results in four parts for comparison. In the translation region, because the polarizability does not change much, the strong group of H-bond vibrations disappears in the IR and Raman spectrum. All phonons herein can be seen from the PDOS curve. The two groups are not particularly regular due to mixing with CH_4 vibrational modes. Li *et al* [29] first noted in 1989 that many

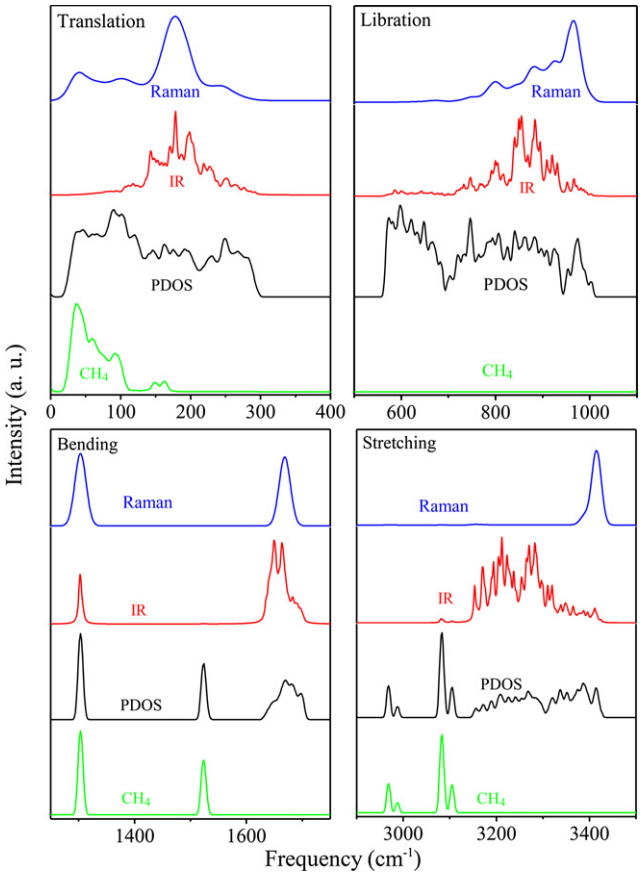

Figure 1. Simulated vibrational spectra of sI gas hydrates. From top to bottom, Raman, IR, PDOS, and partial PDOS of CH_4.

Table 1. Comparisons of some typical peaks with those in the literature, including theoretical calculation and Raman experimental data. All units are cm^{-1}.

	PDOS	INS	IR/Raman (this work)	Theoretical calculation (literature)	Raman experiment data
Weak H-bond	210	208[a]	178/179	217[b]	206[c]
Strong H-bond	291	294[a]			
CH_4 bending	1303		1302/1303	1315[d]/1316–1344[e]/1400>[f]/1254[g]	
CH_4 rocking	1523			1526[d]/1536–1540[e]/1463[g]	
CH_4 symmetric stretch	2969			2939[d]/2925–2943[e]/3014[f]/2871[g]	2915[h]/2915[i]/2913[j]
CH_4 asymmetric stretch	3083			3071[d]/3021–3059[e]/3167[f]/2976[g]	

[a]Reference [41], [b]Reference [42], [c]Reference [19], [d]Reference [23], [e]Reference [43], [f]Reference [22], [g]Reference [49], [h]Reference [16], [i]Reference [44], [j]Reference [45]

ice phases have two main H-bond peaks. Li and Ross [30] suggested that ice has two different H-bond strengths; however, this model has not been widely accepted [31–33]. In 2017, we found two intrinsic H-bond vibrational modes in ice Ic [34]. For one H_2O molecule in an ice Ic lattice, the strong mode includes vibration of four linked H-bonds along the bisector of the HOH angle, which is called a four-bond mode. In the weak mode, only two H-bonds vibrate while the other two remain almost stationary, which is called a two-bond mode. Later, we found that these two kinds of H-bond vibrational modes that comprise the two main peaks in the translation region are a general rule among ice phases [34–40], and we proved that this originated from the local tetrahedral structure of ice [25]. Regarding the hydrogen-ordered ice Ic as the ideal model, the vibrational frequency ratio of these two modes is $\sqrt{2}$.

According to the simulated normal modes of H-bonds in clathrate ice in this work, the strongest frequency of the four-bond mode is at 291 cm^{-1}, and we selected a typical two-bond mode at 210 cm^{-1} for comparison. Figure 2 illustrates the vibration processes of these two modes. (For the dynamic processes, please see the supplementary material.) Celli *et al* [41] reported inelastic neutron scattering (INS) experiments of various clathrate hydrates. For their sI structure, the guest molecule was xenon, so the PDOS curve came mainly from phonons of ice. Two sharp peaks could be seen at 294 and 208 cm^{-1}. The revised

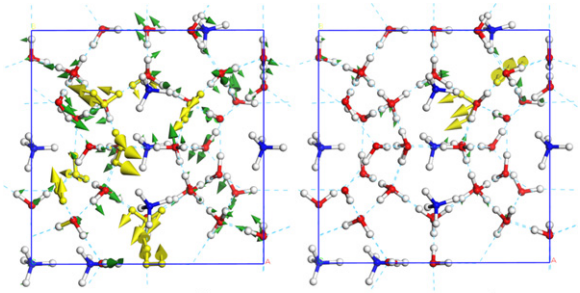

Figure 2. Two examples of H-bond vibration modes. Typical molecules are shown in gold. The oxygen atoms are in red and the carbon atoms are in blue. Wavenumber at 210 cm^{-1} is a two-bond mode, and wavenumber at 291 cm^{-1} is a four-bond mode.

Table 2. Comparisons of sI average structural parameters with experiments and ice XVII.

System	*r*(H–O) (Å)	*r*(C–H) (Å)	*r*(O–H) (Å)	Angle (HCH) (°)	Angle (HOH) (°)
sI (exp.)	1.772[a]	1.098/1.148[b]	1.015[a]	109.5[a]	—
sI (cal.)	1.871	1.094/1.092	0.983	109.4	104.7–107.5
Ice XVII	1.827[c]	—	0.988[c]	—	105–107.9[c]

[a]Reference [46], [b]Reference [22], [c]Reference [47]

Perdew–Burke–Ernzerhof functional slightly underestimates the hydrogen bonding, so our simulated H-bond length is greater than that from the experiment by Klapproth [46]. Table 2 shows that the calculated average length of the H-bonds is 1.871 Å, which is 5.6% greater than the 1.772 Å length from the experimental measurement.

The translational region includes a dormant Raman peak at 179 cm^{-1}, and only one obvious IR peak at 178 cm^{-1}. These results are consistent with experiments in which the strong H-bond peak was difficult to detect with a photon-scattering method [30]. Schicks *et al* [19] presented a Raman scattering peak at 206 cm^{-1} in this region. Tse *et al* [42] used the Perdew–Burke–Ernzerhof generalized gradient approximation functional to propose a peak at 217 cm^{-1}. To verify the effects of the guest molecules, methane, the partial PDOS of CH_4 is presented in figure 1. In the translation region, the main contributions of methane are below 180 cm^{-1}. Because no H-bonds exist between clathrate ice and methane, most of the phonons in this region come from the H-bonds of ice.

Ice XVII, a kind of sI-type clathrate ice structure, was investigated in our previous study, and its vibrational spectrum is presented in figure 3 for comparison [47]. The two triangle peaks of ice XVII are obvious, similar to ice Ih [30]. However, they are less apparent in the sI structure due to mixing with guest molecules.

We compare the INS spectra of sI and liquid water in the far-IR region in figure 4 [41, 48]. The spectrum of sI has two main H-bond peaks at approximately 26–37 meV [31]. However, no such H-bond vibration modes are found in liquid water because it lacks a rigid tetrahedral structure. For liquid water, the strength of molecular rotation modes is lower and leaves an only weak absorption valley in this area. We discovered this phenomenon by comparing liquid water and ice Ih [25]. Although the H-bond absorption band in sI has a slight redshift relative to ice Ih, one can see that the obvious H-bond vibrational frequencies of clathrate ice in sI gas hydrates also fall in the valley of liquid water. The application of terahertz radiation in this area to decompose gas hydrates in water surroundings may be an efficient method. This study further confirms our previous suggestion for energy resource exploitation [25].

As shown in figure 1, the spectrum of the region of libration shows three groups due to the three types of molecular rotation modes: rocking (highest peak, 598 cm^{-1}), wagging (highest peak, 745 cm^{-1}), and twisting (highest peak, 975 cm^{-1}). The encapsulated CH_4 molecules do not contribute any phonons in this band. The simulated PDOS herein agrees well with ice XVII, as shown in figure 3. In contrast, the simulated Raman peaks only manifest one group, the main peak is found at 963 cm^{-1}. And the simulated IR spectrum only shows the wagging band, and the highest absorption peak is found at 854 cm^{-1}.

The third part in figure 1 shows the intramolecular bending modes of CH_4 and H_2O. The two weak peaks at 1303 and 1523 cm^{-1} are CH_4 bending and rocking modes, which agrees well with previous reports [22, 23, 43–45, 49, 50]. There are 25 modes at around 1303 cm^{-1}. Figure 5(a) shows one of the vibrational modes at 1303 cm^{-1}, where the four hydrogens in the gold-colored molecule vibrate in the same direction,

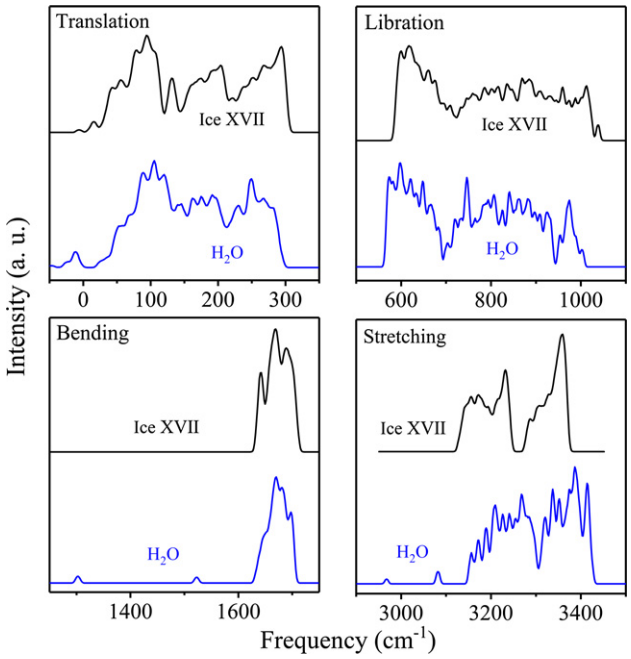

Figure 3. Comparison between sI water clathrates and ice XVII. Ice XVII is a kind of sI clathrate ice without guest molecules and methane molecules encapsulated in the sI structure.

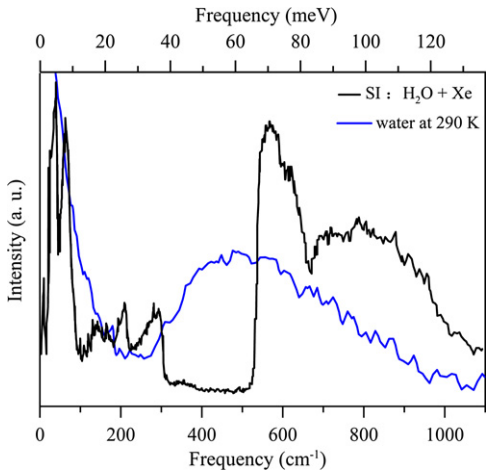

Figure 4. Comparison of translation band of sI gas hydrates [41] (the guest molecule is xenon) and liquid water [48]. H-bond absorption ranges from 20 to 40 meV.

which can be named CH_4 bending. In contrast, the 16 modes around 1523 cm^{-1} are CH_4 rocking modes. Due to limited change in the dipole moment and polarizability for a CH_4 molecule, the intensity of mode at 1523 cm^{-1} is very weak for both Raman and IR spectra. However, Chazallon *et al* [44, 45] observed an overtone at 3053 cm^{-1} and is corresponding to CH_4 rocking. Another overtone at 2570 cm^{-1} was assigned to bending of methane [44, 50]. For the CH_4 bending modes, the changes in vibrational strength within cages of various sizes are very limited. The wavenumbers from 1619 to 1716 cm^{-1} are the bending modes of H_2O. For any IR or Raman spectrum, the peaks are too small to be detected experimentally. The strengths of H_2O bending are also remained stable in various ice phases, and figure 3 shows that the band width is nearly the same as that of ice XVII.

The PDOS curve for the CH_4 stretching band ranges from 2950 to 3125 cm^{-1}. The stronger peaks correspond to asymmetric stretching, and the weaker peaks correspond to symmetric stretching. Both bands show obvious splitting due to the two cage sizes. Compared with the high intensities of OH stretching, these peaks are nearly invisible in the Raman and IR spectra. Table 1 summarizes the CH_4 stretching modes from the simulations and experiments. The calculated CH average bond length is 1.094 cm^{-1}, which is 3.7% shorter than the experimental value [22] of 1.136 cm^{-1}. Inconsistent with the

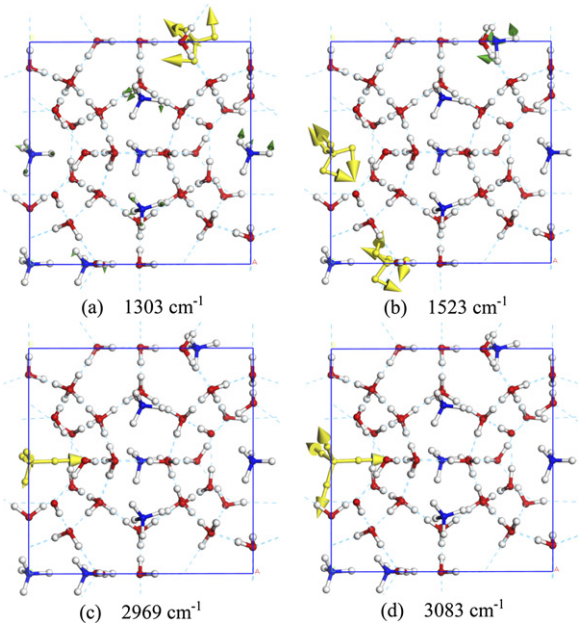

Figure 5. Four examples of vibration normal modes of encapsulated methane. Wavenumbers at 1303 and 1523 cm^{-1} are bending and rocking. Wavenumbers at 2969 and 3083 cm^{-1} are symmetric stretching and asymmetric stretching.

literature [16, 17], the splitting of the CH_4 stretching mode is 20 cm^{-1} for the two sizes of cages. This observation is in accord with simulations from Atilhan *et al* [51] and Hiratsuka *et al* [49]. The splitting of the CH_4 stretching band is related to the difference of the CH bond length in the large and small cages.

The vibration band from 3144 to 3416 cm^{-1} represents OH stretching, as shown in the fourth part of figure 1. The IR spectrum shows two very active peaks at 3211 and 3282 cm^{-1}, which represent more symmetric stretching. However, the strongest Raman peak is at 3415 cm^{-1}, which represents asymmetric stretching modes. As shown in table 2, the OH bond length of sI is shorter than that of ice XVII so that the intramolecular OH stretching band presents a 40 cm^{-1} blueshift, as shown in figure 3, so the wavenumbers of the sI H-bonds have a redshift from ice XVII.

4. Conclusions

Based on the first-principles density functional theory method, we calculated the normal modes of sI gas hydrates, and the simulated Raman scattering and IR absorption spectra are presented for comparison. Because INS experiments can detect phonons throughout the reduced Brillouin zone, previous INS results can be compared with our PDOS curve integrated by $\omega(q)$ dispersions. With good agreement with the literature, we focused on the H-bonds in the far-IR molecular translation band. Although the two groups of H-bonds of clathrate ice do not present two distinct triangle shapes such as in ice XVII, we can still confirm that the phonons in this region come from two kinds of H-bond vibration modes. Because the contributions of CH_4 in this area are below 180 cm^{-1}, we confirm that the effects of methane on these two main peaks are negligible.

The interactions between methane and water cages can be ignored in all regions except the far-IR region. We observed similarities between sI and ice XVII. For the phonons of methane, the splitting of CH stretching can be observed due to the influence of differences in cage size.

We have proposed a new method to decompose gas hydrates via direct application of terahertz radiation to the H-bonds. After a comparison with the partial PDOS of CH_4 in this band, we confirmed that the CH_4 molecules do not absorb this energy. Further experimental measurements are needed.

Acknowledgments

We would like to thank the National Natural Science Foundation of China (Grant No. 11075094). The numerical calculations were done on the supercomputing system in the Supercomputing Center, Shandong University, Weihai.

ORCID iDs

Ying-Bo Lu https://orcid.org/0000-0001-7799-8751
Peng Zhang https://orcid.org/0000-0002-1099-6310

References

[1] Sloan E D 1998 Gas hydrates: review of physical/chemical properties *Energy Fuels* **12** 191–6
[2] Lunine J I and Stevenson D J 1987 Clathrate and ammonia hydrates at high pressure: application to the origin of methane on Titan *Icarus* **70** 61–77
[3] Takeya S *et al* 2011 Nondestructive imaging of anomalously preserved methane clathrate hydrate by phase contrast x-ray imaging *J. Phys. Chem.* C **115** 16193–9
[4] Englezos P 1993 Clathrate hydrates *Ind. Eng. Chem. Res.* **32** 1251–74
[5] O'Connor F M *et al* 2010 Possible role of wetlands, permafrost, and methane hydrates in the methane cycle under future climate change: a review *Rev. Geophys.* **48 RG4005**
[6] Konno Y, Masuda Y, Akamine K, Naiki M and Nagao J 2016 Sustainable gas production from methane hydrate reservoirs by the cyclic depressurization method *Energy Convers. Manage.* **108** 439–45
[7] Dickens G R and Quinby-Hunt M S 1994 Methane hydrate stability in seawater *Geophys. Res. Lett.* **21** 2115–8
[8] Muller H and von Stackelberg M 1951 On the structure of gas hydrates *J. Chem. Phys.* **19** 1319–20
[9] Kvenvolden K A 1995 A review of the geochemistry of methane in natural gas hydrate *Org. Geochem.* **23** 997–1008
[10] Hoshikawa A, Igawa N, Yamauchi H and Ishii Y 2006 Observation of hydrogen in deuterated methane hydrate by maximum entropy method with neutron powder diffraction *J. Chem. Phys.* **125** 034505
[11] Sloan E D 2003 Clathrate hydrate measurements: microscopic, mesoscopic, and macroscopic *J. Chem. Thermodyn.* **35** 41–53
[12] Efimchenko V S, Kuzovnikov M A, Fedotov V K, Sakharov M K, Simonov S V and Tkacz M 2011 New phase in the water–hydrogen system *J. Alloys Compd.* **509** S860–3
[13] Strobel T A, Somayazulu M and Hemley R J 2011 Phase behavior of $H_2 + H_2O$ at high pressures and low temperatures *J. Phys. Chem.* C **115** 4898–903
[14] Sloan E D 2003 Fundamental principles and applications of natural gas hydrates *Nature* **426** 353–9
[15] Anthonsen J 1975 The Raman spectra of some halogen gas hydrates *Chem. Informationsdienst* **6** 175–8
[16] Sum A K, Burruss R C and Sloan E D 1997 Measurement of clathrate hydrates via Raman spectroscopy *J. Phys. Chem.* B **101** 7371–7
[17] Greathouse J A, Cygan R T and Simmons B A 2006 Vibrational spectra of methane clathrate hydrates from molecular dynamics simulation *J. Phys. Chem.* B **110** 6428–31
[18] Kortus J, Irmer G, Monecke J and Pederson M R 2000 Influence of cage structures on the vibrational modes and Raman activity of methane *Modelling Simul. Mater. Sci. Eng.* **8** 403
[19] Schicks J M, Erzinger J and Ziemann M A 2005 Raman spectra of gas hydrates-differences and analogies to ice 1h and (gas saturated) water *Spectrochim. Acta* A **61** 2399–403
[20] Hansen S B and Berg R W 2009 Raman spectroscopic studies of methane gas hydrates *Appl. Spectrosc. Rev.* **44** 168–79
[21] Tulk C A, Ripmeester J A and Klug D D 2000 The application of Raman spectroscopy to the study of gas hydrates *Ann. New York Acad. Sci.* **912** 859–72
[22] John S T 2002 Vibrations of methane in structure I clathrate hydrate—an *ab initio* density functional molecular dynamics study *J. Supramol. Chem.* **2** 429–33
[23] Ramya K R, Pavan Kumar G V and Venkatnathan A 2012 Raman spectra of vibrational and librational modes in methane clathrate hydrates using density functional theory *J. Chem. Phys.* **136** 174305
[24] Del Rosso L, Celli M and Ulivi L 2016 New porous water ice metastable at atmospheric pressure obtained by emptying a hydrogen-filled ice *Nat. Commun.* **7** 13394
[25] Zhu X-L, Cao J-W, Qin X-L, Jiang L, Gu Y, Wang H-C, Liu Y, Kolesnikov A I and Zhang P 2020 Origin of two distinct peaks of ice in the THz region and its application for natural gas hydrate dissociation *J. Phys. Chem.* C **124** 1165–70
[26] Clark S J, Segall M D, Pickard C J, Hasnip P J, Probert M I, Refson K and Payne M C 2005 First principles methods using CASTEP *Z. Kristallogr.* **220** 567–70
[27] Matsumoto M, Yagasaki T and Tanaka H 2018 GenIce: hydrogen-disordered ice generator *J. Comput. Chem.* **39** 61–4
[28] Hammer B, Hansen L B and Nørskov J K 1999 Improved adsorption energetics within density-functional theory using revised Perdew–Burke–Ernzerhof functionals *Phys. Rev.* B **59** 7413
[29] Li J, Ross D, Howe L, Hall P and Tomkinson J 1989 Inelastic incoherent neutron scattering spectra of single crystalline and polycrystalline ICE Ih *Physica* B **156–157** 376–9
[30] Li J and Ross D 1993 Evidence for two kinds of hydrogen bond in ice *Nature* **365** 327–9
[31] John S T and Klug D D 1995 Comments on 'Further evidence for the existence of two kinds of H-bonds in ice Ih' by Li *et al Phys. Lett.* A **198** 464–6
[32] Morrison I and Jenkins S 1999 First principles lattice dynamics studies of the vibrational spectra of ice *Physica* B **263–264** 442–4
[33] Klotz S, Strässle T, Salzmann C, Philippe J and Parker S 2005 Incoherent inelastic neutron scattering measurements on ice VII: are there two kinds of hydrogen bonds in ice? *Europhys. Lett.* **72** 576
[34] Yuan Z-Y, Zhang P, Yao S-K, Lu Y-B, Yang H-Z, Luo H-W and Zhao Z-J 2017 Computational assignments of lattice vibrations of ice Ic *RSC Adv.* **7** 36801–6
[35] Zhang P, Wang Z, Lu Y B and Ding Z W 2016 The normal modes of lattice vibrations of ice XI *Sci. Rep.* **6** 29273
[36] Yao S-K, Zhang P, Zhang Y, Lu Y-B, Yang T-L, Sun B-G, Yuan Z-Y and Luo H-W 2017 Computing analysis of lattice vibrations of ice VIII *RSC Adv.* **7** 31789–94
[37] Jiang L, Yao S K, Zhang K, Wang Z R, Luo H W, Zhu X L, Gu Y and Zhang P 2018 Exotic spectra and lattice vibrations of ice X using the DFT method *Molecules* **23 2780**
[38] Cao J W, Chen J Y, Qin X L, Zhu X L, Jiang L, Gu Y, Yu X H and Zhang P 2019 DFT investigations of the vibrational spectra and translational modes of ice II *Molecules* **24 3135**
[39] Gu Y, Zhu X-L, Jiang L, Cao J-W, Qin X-L, Yao S-K and Zhang P 2019 Comparative analysis of hydrogen bond vibrations in ice VIII and VII *J. Phys. Chem.* C **123** 14880–3

[40] Qin X L, Zhu X L, Cao J W, Jiang L, Gu Y, Wang X C and Zhang P 2019 Computational analysis of exotic molecular and atomic vibrations in ice XV *Molecules* **24** 3115
[41] Celli M, Colognesi D, Ulivi L, Zoppi M and Ramirez-Cuesta A J 2012 Phonon density of states in different clathrate hydrates measured by inelastic neutron scattering *J. Phys.: Conf. Ser.* **340 012051**
[42] Tse J S, Klein M L and McDonald I R 1983 Molecular dynamics studies of ice Ic and the structure I clathrate hydrate of methane *J. Phys. Chem.* **87** 4198–203
[43] Uchida T, Ohmura R and Hori A 2010 Raman peak frequencies of fluoromethane molecules measured in clathrate hydrate crystals: experimental investigations and density functional theory calculations *J. Phys. Chem.* A **114** 317–23
[44] Chazallon B, Focsa C, Charlou J-L, Bourry C and Donval J-P 2007 A comparative Raman spectroscopic study of natural gas hydrates collected at different geological sites *Chem. Geol.* **244** 175–85
[45] Bourry C *et al* 2009 Free gas and gas hydrates from the Sea of Marmara, Turkey: chemical and structural characterization *Chem. Geol.* **264** 197–206
[46] Klapproth A 2002 *Doctoral dissertation* Georg-August-University, Göttingen, Germany
[47] Zhu X-L *et al* 2019 Computational analysis of vibrational spectrum and hydrogen bonds of ice XVII *New J. Phys.* **21** 043054
[48] Wang Y and Dong S 2003 Neutron scattering studies of low-fraction H_2O in silica gel *Phys. Rev.* B **68** 172201
[49] Hiratsuka M, Ohmura R, Sum A K and Yasuoka K 2012 Molecular vibrations of methane molecules in the structure I clathrate hydrate from *ab initio* molecular dynamics simulation *J. Chem. Phys.* **136** 044508
[50] Hachikubo A *et al* 2012 Raman spectroscopic and calorimetric observations on natural gas hydrates with cubic structures I and II obtained from Lake Baikal *Geo-Mar. Lett.* **32** 419–26
[51] Atilhan M, Pala N and Aparicio S 2014 A quantum chemistry study of natural gas hydrates *J. Mol. Model.* **20** 2182